PERGAMON

Available online at www.sciencedirect.com

SCIENCE DIRECT®

Electrochimica Acta 48 (2003) 1031–1039

ELECTROCHIMICA Acta

www.elsevier.com/locate/electacta

Synthesis and electrochemical characterization of orthorhombic $LiMnO_2$ material

Y.S. Lee [a], Y.K. Sun [b], K. Adachi [a], M. Yoshio [a,*]

[a] *Department of Applied Chemistry, Saga University, 1 Honjo, Saga 840-8502, Japan*
[b] *Department of Chemical Engineering, Hanyang University, Seoul 133-791, South Korea*

Received 2 October 2002; received in revised form 9 December 2002

Abstract

Well-defined orthorhombic $LiMnO_2$ was synthesized using LiOH and γ-MnOOH starting materials at 1000 °C in an argon flow by quenching process. X-ray diffraction (XRD) revealed that the compound showed an orthorhombic phase of a space group with *Pmnm* ($a = 2.806$ Å, $b = 5.750$ Å, and $c = 4.593$ Å). The prepared compound was composed of particles of about 5–15 μm diameter with a bar-shape and small spherical one of about 1–2 μm. It showed very small initial discharge capacity of about 34 mA h g^{-1} in the (3+4) V region at room temperature. However, after 12 h grinding, the $LiMnO_2$ delivered 201 mA h g^{-1} in the first cycle and still delivered 200 mA h g^{-1} after 50 cycles at room temperature. We found that the initial discharge capacity of $LiMnO_2$ agreed well with its specific surface area by Brunauer, Emmett and Teller (BET) analysis. Especially, the grinding treatment played an important role to activate the lithium insertion–extraction into the $LiMnO_2$ layer in the 3 V region.

Keywords: Orthorhombic; $LiMnO_2$; Quenching; Structural change; Grinding effect

1. Introduction

The battery industries have aimed to supply safe power sources with high energy density and good cycle performance. Lithium secondary batteries are the most promising candidate among the many possibilities to satisfy this demand [1–3].

Layered lithium metal oxide with the general formula $LiMO_2$ (M = Co, Ni, Mn) has a rock salt structure where lithium and transition metal cation occupy alternate layers of octahedral sites in a distorted close-packed oxygen ion lattice. The layered MO_2 framework provides two-dimensional interstitial spaces which allows easy extraction of lithium ions [4–6]. It was known that $LiMnO_2$ structure with an almost ideal layered arrangement of the lithium and manganese ions could be prepared Li^+ ion-exchange from α-$NaMnO_2$. According to the synthetic condition and mechanism, $LiMnO_2$ forms an orthorhombic unit cell with a space group *Pmnm* ($a = 2.805$ Å, $b = 5.757$ Å, and $c = 4.527$ Å) and a monoclinic unit cell with a space group *C*/2*m* ($a = 5.439$ Å, $b = 2.809$ Å, and $c = 5.388$ Å) [7,8]. Furthermore, a second polymorph of $LiMnO_2$ has been prepared by chemical lithiation of the spinel $Li_2Mn_2O_4$. A tetragonal cell was indicated with $a = 5.662$ Å and $c = 9.274$ Å (*I*41/*amd*, $Z = 8$) [9].

Since orthorhombic $LiMnO_2$ (herein referred to as *o*-$LiMnO_2$) with the ordered rock salt structure was revealed by Johnston and Keikes, many research groups reported lots of new synthetic processes to obtain a well-defined *o*-$LiMnO_2$ with an excellent cycling performance [10,11]. Some research groups have reported many interesting characteristics of *o*-$LiMnO_2$; such as the relation between grain size and discharge capacity, some impurities that may enhance the electronic conductivity of *o*-$LiMnO_2$ structure and the phase transformation from orthorhombic to spinel structure, which could be a main reason of capacity decline of Li/$LiMnO_2$ cell [12–24].

Recently, we reported a new synthetic method using quenching process, which could synthesize a well-crystallized *o*-$LiMnO_2$ material at 1000 °C by one-step

* Corresponding author. Tel.: +81-952-28-8673; fax: +81-952-28-8591.
E-mail address: yoshio@ccs.ce.saga-u.ac.jp (M. Yoshio).

0013-4686/02/$ - see front matter © 2002 Elsevier Science Ltd. All rights reserved.
doi:10.1016/S0013-4686(02)00817-4

method [25]. This work showed a couple of new indications as follows; first, the unique quenching effect for obtaining the pure orthorhombic $LiMnO_2$ phase, which showed no structural transformation to the spinel-like phase during the cooling process. Second, o-$LiMnO_2$ material with an excellent cycling performance at room and high temperature (55 °C) could be obtained easily without the exchange reaction of Li^+/Na^+ or maintaining the sensitive synthetic condition. Last, it clearly revealed the marvelous relation between particle size (or surface area) and initial discharge capacity of o-$LiMnO_2$ compound by adopting the grinding process.

Most recently, we found an interesting grinding mechanism of improved discharge capacity for Li/$LiMnO_2$ cell and succeeded to optimize the cell performance at room temperature, which showed almost no capacity decline until 50 cycles. Moreover, we did not present other more interesting electrochemical characteristics for the o-$LiMnO_2$ powder in previous report [25]. Therefore, we report here the synthetic procedure of o-$LiMnO_2$ in detail and present the unique electrochemical characterizations of o-$LiMnO_2$, especially the grinding role and effect before and after grinding.

2. Experimental

The orthorhombic $LiMnO_2$ material was synthesized using $LiOH{\cdot}H_2O$ (Osaka Kisida Chemical, Japan) and γ-MnOOH (Tosoh Chemical, Japan). The mixture of LiOH and γ-MnOOH (molar ratio of Li/Mn = 1.02) was thoroughly ground in an agate mortar. A small amount of lithium was added to compensate for lithium evaporation at high temperature during the calcination process. The mixture was pressed at a 300 kg cm^{-2} pressure into a 25 mm diameter pellet to improve the reactivity between particles of the precursor. After calcinations at 950–1100 °C for 10 h under argon flow, it was taken from the box-furnace and rapidly cooled in air without any treatment.

The thermal decomposition behavior of the precursors was examined by means of thermogravimetric analysis and differential thermal analysis using a TG-8110 thermal analyzer system (TGA, DTA, TAS 100, Rigaku Ltd., Japan). The heating–cooling rate was 5 °C min^{-1}. The powder X-ray diffraction (XRD, Rint 1000, Rigaku, Japan) using CuKα radiation was employed to identify the crystalline phase of the synthesized materials. The lithium and manganese concentrations in the resulting materials were analyzed using an inductively coupled plasma spectrometer (ICP, SPS 7800, Seiko Instruments, Japan). The specific surface area was measured in a Gemini 2375 instrument using the Brunauer, Emmett and Teller (BET) method. The particle morphologies of the resulting compound were observed using a scanning electron microscope (SEM, JSM-5300E, Japan Electron, Ltd., Japan) and a transmission electron microscopy (TEM, JEM2010, JEOL, Japan).

In the case of average oxidation state of Mn in synthesized compound, titration with excess $FeSO_4$ solution with standard $KMnO_4$ solution was carried out. The total Mn ion was determined by a complexometric titration method, in which excess EDTA was analyzed by back titration using standard zinc solution. The sample was first dissolved in hydroxylammonium chloride solution containing EDTA in advance. To quantitatively measurement the oxygen content in two compounds, an oxygen determination analyzer (RO-416DR, EF-40C, LECO Corporation, USA) was used for the oxygen analysis.

A three-electrode glass cell was used for cyclic voltammetry (CV) measurement. The working electrode was consisted of 3 mg of the active material and 2.2 mg of conducting binder (Teflonized acetylene black (TAB)), which was pressed onto stainless steel mesh. The counter and reference electrodes were prepared by pressing lithium foil onto stainless steel gauze. The CV measurement was performed with an Arbin Instruments Model MSTAT4 battery test system at 0.2 mV s^{-1} scan rate between the voltage limits of 2.0–4.5 V. All assembling of the cell was carried out in a dry box filled with argon gas.

The electrochemical characterizations were performed using CR2032 coin-type cells. The cathode was fabricated with 20 mg of accurately weighed active material and 12 mg of conductive binder (8 mg of TAB and 4 mg of graphite). It was pressed on a 250 mm^2 stainless steel mesh used as the current collector at a pressure of 300 kg cm^{-2} and dried at 200 °C for 5 h in an oven. The test cell was made of a cathode and a lithium metal anode (Cyprus Foote Mineral Co.) separated by a porous polypropylene film (Celgard 3401). The electrolyte used was a mixture of 1 M $LiPF_6$-ethylene carbonate (EC)–dimethyl carbonate (DMC) (1:2 by volume) (Ube Chemical, Japan). All the assembling of the cell was carried out in an argon-filled dry box. The charge and discharge cycling was galvanostatically performed at a current density of 0.4 mA cm^{-2} with a cutoff voltage of 2.0–4.5 V (or 2.0–4.3 V for the after grinding) at room (25 °C) and various high temperatures (40–80 °C).

3. Results and discussion

Fig. 1 shows the thermogravimetric analysis of LiOH and γ-MnOOH mixture. The mixture was heated at 5 °C min^{-1} and cooled at 5 °C min^{-1} in Ar flow. It exhibited four significant endothermic peaks on the DTA curve. The first distinct peak around 80 °C is due to the removal of water from $LiOH{\cdot}H_2O$. The second peak at

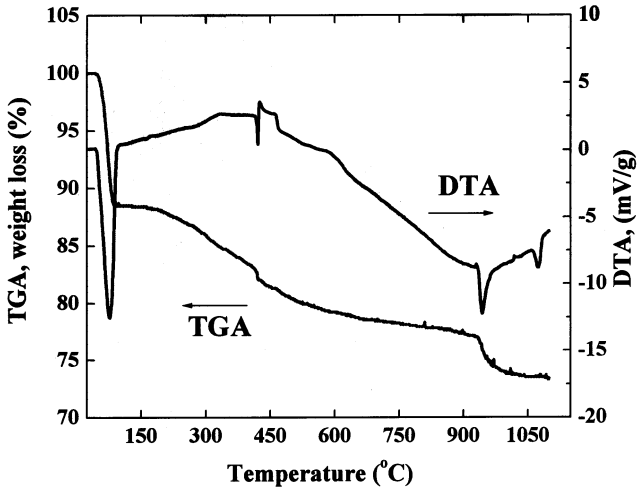

Fig. 1. The mogravimetric and differential thermal analyses for precursor which was $LiOH \cdot H_2O$ mixed with γ-MnOOH. The mixture was dried in a vacuum oven at 25 °C prior to the thermal analysis and the heating rate was 5 °C min^{-1} under an Ar flow.

420 °C is expected to the formation of the disordered $LiMn_2O_{4+y}$ spinel. It is well known that some impurities of β-MnO_2, which is converted from γ-MnOOH at 260 °C, still remained with the disordered $LiMn_2O_{4+y}$ spinel in this region [26]. The third DTA peak reveals that there is another reaction at 950 °C that may be the conversion from the $LiMn_2O_4$ spinel phase to the orthorhombic $LiMnO_2$ compound. The XRD pattern of LiOH and γ-MnOOH obtained at 900 °C (Fig. 2a) by quenching shows a similar to that of an orthorhombic (Fddd) phase of $LiMn_2O_4$, which changed from cubic $LiMn_2O_4$ spinel at low temperature (−23 °C) [27,28]. It means that the mixture of LiOH and γ-MnOOH still maintained a $LiMn_2O_4$ spinel type structure at 900 °C and it changed into the orthorhombic $LiMnO_2$ during the third enthothermal process at about 950 °C. We believe that this result could be a good clue to understanding for the synthesis of orthorhombic $LiMnO_2$ material by quenching process. The formed $LiMnO_2$ phase at over 950 °C was well crystallized in the

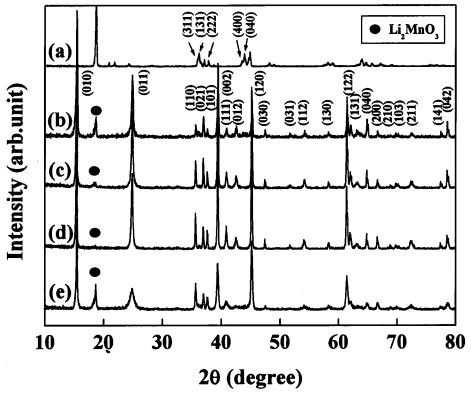

Fig. 2. XRD patterns of $LiMnO_2$ material (a) 900 °C, (b) 950 °C, (c) 1000 °C, (d) 1050 °C and (e) 1100 °C.

temperature region of 1000–1050 °C. We suspect that the last DTA peak at about 1070 °C might result from the decomposition of $LiMnO_2$ phase or the transformation of small Li_2MnO_3 impurity in the $LiMnO_2$ powder.

From the thermogravimetric analysis, we expected that *o*-$LiMnO_2$ could be obtained from the calcination temperature range of 950–1100 °C. Additionally, we already reported that the quenching process could preserve its original $LiMnO_2$ structure, which prevented structural transformation to the spinel-like phase during cooling process [25]. Fig. 2 shows the XRD pattern of the $LiMnO_2$ material calcined at different temperatures. For calcination temperature $T < 950$ °C, it showed mixed structure patterns with a cubic, orthorhombic of $LiMn_2O_4$ and a small amount of tetragonal $Li_2Mn_2O_4$ phases in the XRD diagram. However, when the calcination temperature is above 950 °C (Fig. 2b), the (010) peak at $2\theta = 15.3°$ rapidly increased and other peaks also indicated a major phase of the *o*-$LiMnO_2$ material. For the 1050 °C sample (Fig. 2d), it exhibited a pure XRD pattern without any other impurities and a very small amount of the Li_2MnO_3 phase. On the other hand, the 1100 °C sample presented a quite different XRD pattern with a strong Li_2MnO_3 impurity peak and a smaller (011) peak. Table 1 shows the various powder characteristics of $LiMnO_2$ materials at different calcination temperatures. The oxidation state of Mn and oxygen content decrease with increasing the calcination temperatures (950–1050 °C). However, the compound at 1100 °C showed fairly different lattice constants and high oxidation state compared with those of other materials. Although Croguennec et al. reported a useful concept of (110) line at $2\theta = 24.8°$, which related to the monoclinic stacking fault in orthorhombic $LiMnO_2$ material, we considered that the discussion about (110) line in this study is meaningless because the overall composition of material at 1100 °C was $Li_{0.71}MnO_{1.93}$ and still remained a large amount of Li_2MnO_3 impurity peak in the XRD diagram. Therefore, we considered that the well-ordered *o*-$LiMnO_2$ material in this study was formed at the calcination temperatures of 1000–1050 °C by a quenching, although there was one difference in the intensity ratios of the (110)/(021) and (002)/(120) peaks between 1000 and 1050 °C samples.

To investigate the effect of the gas atmosphere during the calcination process, three kinds of gases (argon, air and oxygen) were used in this experiment. All the synthetic conditions were the same as mentioned above except for the sort of gas. The used furnace was a commercial box-furnace (KDF S70G, Denken, Japan) and each gas was flowed at 500 cm^3 min^{-1} during the heating process. The XRD patterns of three samples under different gas atmospheres were almost the same and exhibited a well-defined $LiMnO_2$ structure at 1000 °C. However, the lattice constants of the $LiMnO_2$ material were slightly different from each other. The

Table 1
Overall properties and chemical analysis of $LiMnO_2$ obtained at various temperatures

Temperature (°C)	Composition	a (Å)	b (Å)	c (Å)	Oxidation state of Mn
950	$LiMnO_{2.02}$	2.805	5.751	4.572	3.067
1000	$Li_{0.99}MnO_{2.02}$	2.806	5.750	4.594	3.053
1050	$Li_{0.99}MnO_{1.99}$	2.807	5.753	4.577	3.038
1100		2.810	5.749	4.591	3.149

$LiMnO_2$ obtained under an air flow showed the smallest c-axis value (Ar: 4.594 Å, O_2: 4.582 Å, and air; 4.575 Å). Fig. 3 shows the relation of the relative discharge capacity and the gas used during the calcination process. The capacity at each point was standardized to that of the compound obtained under an argon flow ($C_{(air\ or\ O_2)}/C_{Ar} \times 100$). As shown in this figure, the compounds made in air and O_2 showed a small discharge capacity. Furthermore, the compound obtained under air flow showed a dissimilar cycle behavior when compared with the other two materials, especially during the early stage. This means that the argon flow is more desirable for obtaining a well-defined o-$LiMnO_2$ with a high Mn^{3+} fraction by preventing any reaction with oxygen during the calcination process. On the basis of these results, we concluded that the optimum synthetic condition of o-$LiMnO_2$ in this research is the calcination at 1000–1050 °C for 10 h under argon flow and then cooling by the quenching.

Fig. 4 shows the scanning electron micrographs (SEM) for the $LiMnO_2$ compounds calcined at different temperatures. For the 950, 1000 and 1050 °C samples, these consisted of particles of about 5–15 μm diameter with a bar-shape and small spherical one of about 2–3 μm, which is the typical crystallite pattern of the compound using the γ-MnOOH starting material [29,30]. However, the particle size of the 1100 °C sample remarkably increased and the shape of the particles almost changed to the spherical type. Roughly, the particle sizes of all compounds in Fig. 4 were remarkably larger than other results which were obtained using different synthetic methods [14,15,19,22]. Specially, Croguennec et al. [18,19] have suggested the effect of crystallite size on the cycle performance of the $LiMnO_2$ material. They successfully synthesized two kinds of compounds with a small crystallite size (<1 μm) and large crystallite size (<10 μm). They reported an interesting result that the compound with the small grain size showed about twice the discharge capacity of the compound with a large grain size. Since the intercalation of a compound primarily takes place on the grain surface, the $LiMnO_2$ material prefers to have a small grain size to induce the rapid lithium diffusion between the bulk and its surface. Consequently, they proposed that the $LiMnO_2$ material should have a small grain size below about 1 μm to yield the best electrochemical performance. Therefore, we expect that the o-$LiMnO_2$ material in this study will have a small discharge capacity and poor electrochemical characterization due to its large particle size, if it follows their interpretation.

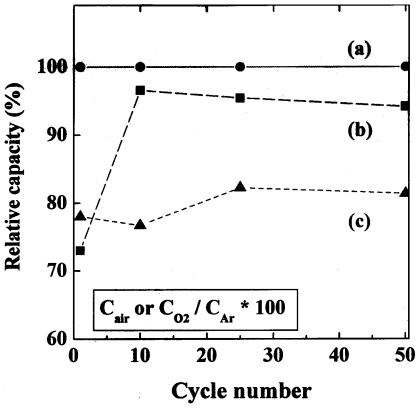

Fig. 3. Relative discharge capacity of $LiMnO_2$ material obtained under different gas flows. (a) Ar, (b) air and (c) O_2.

Fig. 5 shows cycling characteristics of the $LiMnO_2$ electrodes at room and high temperatures. The data were collected at a current density of 0.4 mA cm^{-2} between 4.5 and 2.0 V. The $LiMnO_2$ electrode, which was cycled at room temperature, showed a very small initial discharge capacity of about 34 mA h g^{-1} and a slowly increasing capacity on cycling (Fig. 5a and b). From the point of view for large particle size over 10 μm, it was one interesting fact that this material exhibited almost twice discharge capacity than that of previously reported data by Croguennec et al. [19]. Furthermore, for the high temperature test cell, even if it also showed a small initial discharge capacity during the first cycle, the capacity increased very fast and reached a maximum point during the early stage (Fig. 5c). Chiang et al. also reported a similar result for o-$LiMnO_2$, which exhibited an excellent cycleability under almost the same test condition, however, its discharge capacity continuously decreased and reached about 80 mA h g^{-1} after the 100th cycle [24]. The $LiMnO_2$ compound in this research delivered 186 mA h g^{-1} during the tenth cycle (the maximum value of capacity) and still delivered 176 mA h g^{-1} after 100 cycles. The cycle retention rate is 95%, therefore, it only decreased by 0.1 mA h g^{-1} per cycle in the 3 and 4 V regions.

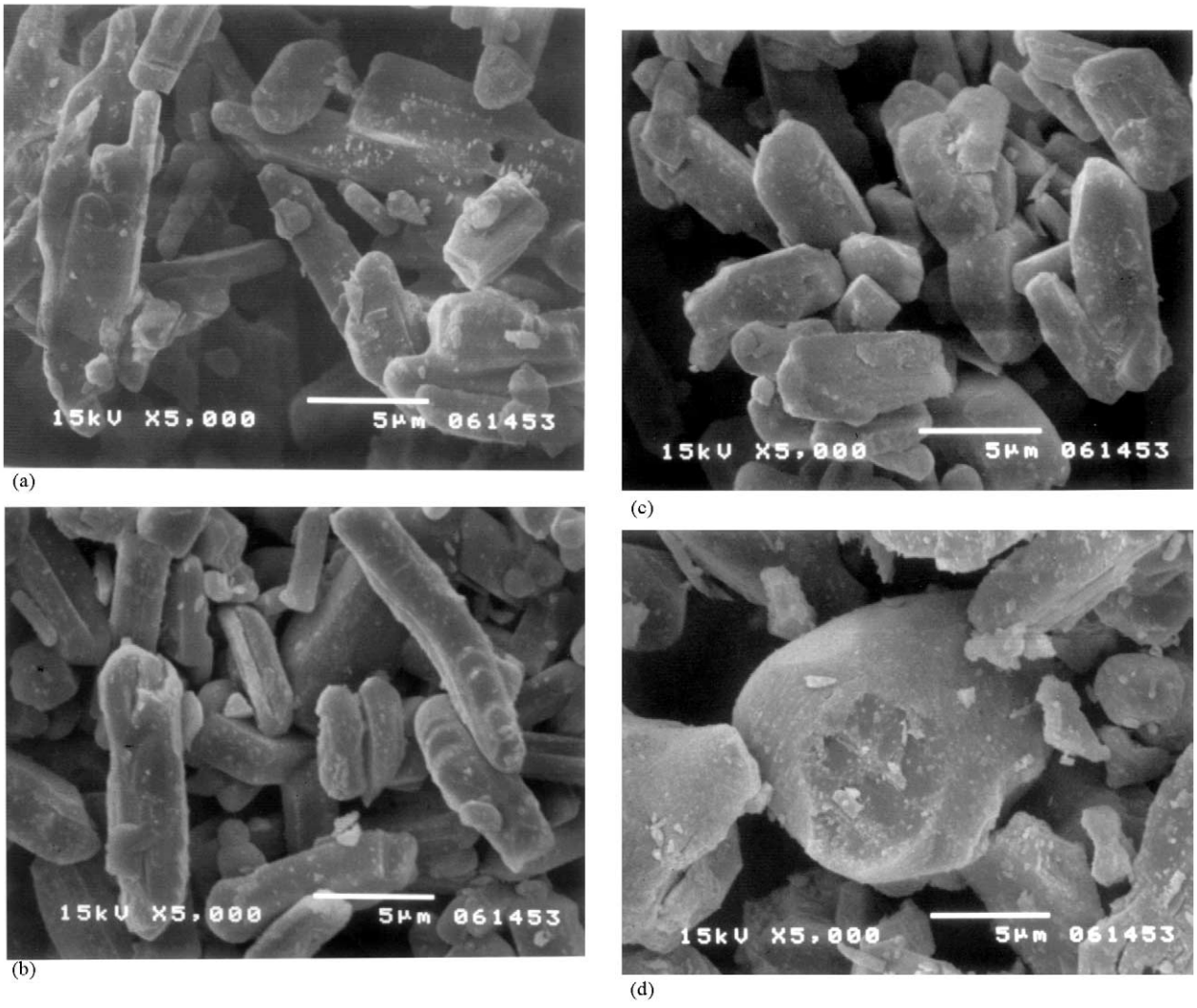

Fig. 4. SEM images of $LiMnO_2$ material (a) 950 °C, (b) 1000 °C, (c) 1050 °C and (d) 1100 °C.

To investigate more closely the relation between the discharge capacity and testing temperature, each Li/$LiMnO_2$ cell was tested at three different temperatures (40, 60, and 80 °C). The initial discharge capacity increased upon increasing the testing temperature as shown in Fig. 6. The capacity of $LiMnO_2$ was linearly increased the test at 40 °C and showed the largest initial discharge capacity of over 214 mA h g^{-1} at 80 °C. This means that there is a wide difference in the amount of lithium ions inserted into the $LiMnO_2$ structure and different rates of reaction occur during the discharge process between room and high temperatures.

Furthermore, Croguennec et al. have reported the effect of the grain sizes for *o*-$LiMnO_2$ on the various discharge capacities as described before [18,19]. Therefore, we assumed that the grinding treatment is very useful way to change the surface area, which can affect the characteristic between electrolyte and particle surface of *o*-$LiMnO_2$ material. Since it showed relatively a large particle size over 10 μm, the grinding treatment smashes it to small particles and increases surface area of the *o*-$LiMnO_2$. Therefore, it makes better contact between the particles and electrolyte and it helps to accelerate the lithium diffusion in the $LiMnO_2$ structure. In order to increase the specific surface area of *o*-$LiMnO_2$ compound, it was thoroughly ground in an agate mortar by a milling machine (ANM 1000, Nito. Co., Japan). The TEM images show the morphology of the *o*-$LiMnO_2$ compound. The compound before grinding is represented in Fig. 7a and the compound after grinding for a 24 h is shown in Fig. 7b. The *o*-$LiMnO_2$ compound before grinding had a typical bar-shaped type as mentioned above. However, the average particle size and shape of $LiMnO_2$ after grinding is surprisingly decreased and changed compared with those of the original $LiMnO_2$. The particle size for the compound after grinding was from 50 to 500 nm. We also could not find the whole bar-shaped type after grinding, which original bar-shape particle of $LiMnO_2$ using γ-MnOOH source. In addition, BET analysis strongly supported

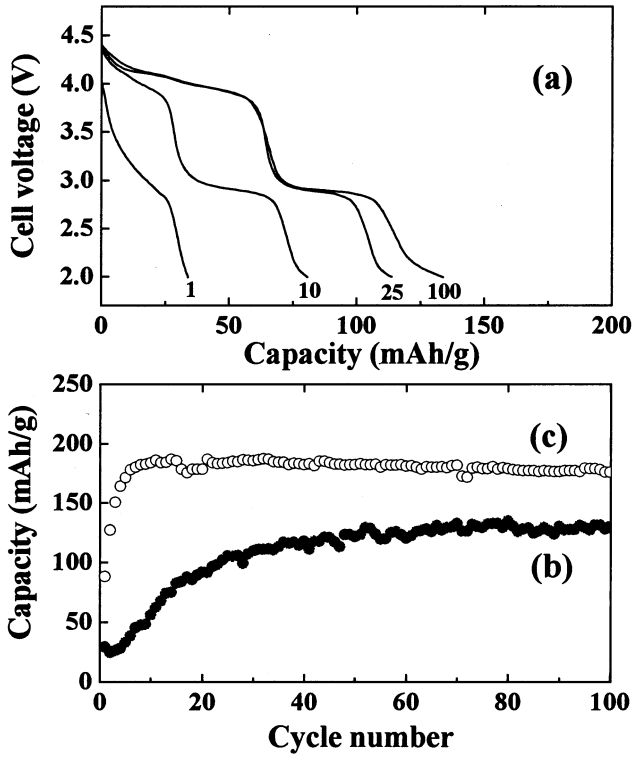

Fig. 5. (a) Discharge curves, (b) specific discharge capacity for Li/1 M $LiPF_6$-EC/DMC/$LiMnO_2$ cell at 25 °C, and (c) 50 °C. Cycling was carried out at a constant charge–discharge current density of 0.4 mA cm^{-2} between 4.5 and 2.0 V.

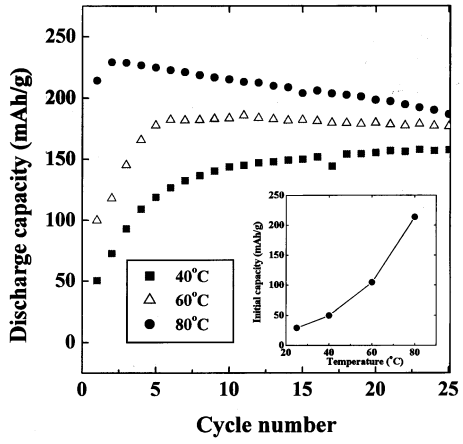

Fig. 6. The plot of specific discharge capacity vs. number of cycles for the Li/1 M $LiPF_6$-EC/DMC/$LiMnO_2$ cells at different high temperatures; (a) 40 °C, (b) 60 °C, and (c) 80 °C. Cycling was carried out at a constant charge–discharge current density of 0.4 mA cm^{-2} between 4.5 and 2.0 V.

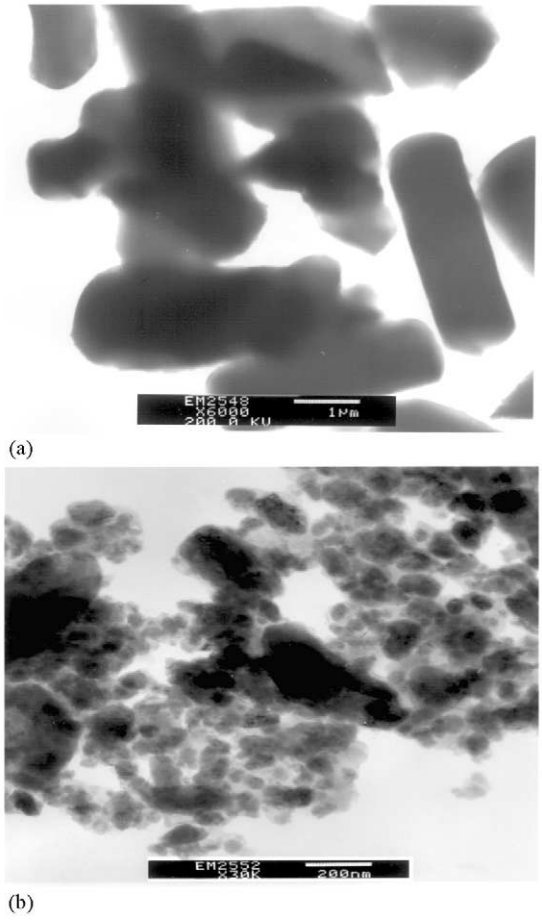

Fig. 7. TEM images of $LiMnO_2$ (a) before grinding, (b) after a 24 h grinding.

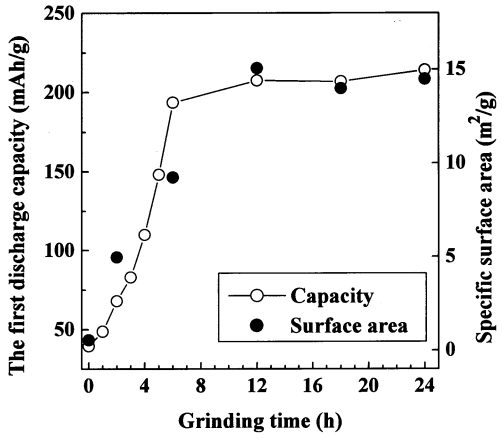

Fig. 8. Dependence of the first discharge capacity and specific surface area of $LiMnO_2$ compounds on the grinding time.

our assumption about grinding effect for $LiMnO_2$ material in this study. Fig. 8 shows the relation between initial discharge capacity and specific surface area of *o*-$LiMnO_2$ compound depends on the grinding time. The surface areas of the two compounds were 0.55 $m^2\ g^{-1}$ before grinding and 14.5 $m^2\ g^{-1}$ after a 24 h grinding, respectively. It is noticeable that the specific surface area after a 24 h grinding was as 26 times as much as that before grinding. Furthermore, the $LiMnO_2$ compound before grinding shows the lowest discharge capacity. However, as the grinding time of the $LiMnO_2$ powder

increased, the initial discharge capacity linearly increased, and then showed the similar capacity compared with that of a 12 h grinding. It suggests that there is a pulverization limit and long-term grinding is useless for increasing surface area beyond this point (the maximum point critically depends on grinding speed and amount of powder). Also, the specific surface area of $LiMnO_2$ well agreed with the amount of discharge capacity.

Fig. 9 exhibits the XRD pattern of the *o*-$LiMnO_2$ materials after grinding at various grinding times (0–24 h). The (010) peak at $2\theta = 15.3^\circ$ in the XRD diagram was slightly moved to the high angle after 6 h grinding. As the grinding time increases, the full width at half maximum (FWHM) of major peaks, (011), (002), (102) and (122), remarkably increases. Although it is well known that the increase of FWHM resulted from a small crystalline size and lattice strain caused by the harsh and long-term grinding [23,33], especially, the two small concrete peaks at $2\theta = 41$–43°, which were (111) and (012) peaks, totally changed and could not detect any more in the same scan position after 12 h grinding. Therefore, we assumed that the $LiMnO_2$ powder after 12 h grinding seems to be changing to the partially amorphous structure, because there are still main peaks, from the high crystalline structure. The similar indication was already reported that the amorphous manganese oxide was possible to be obtained with the higher discharge capacity due to increase the electrical conductivity by ball milling and it exhibited higher lithium intercalation than high crystalline oxide material [31,32]. Therefore, we concluded that the structure of $LiMnO_2$ in this study partially/locally changed into the amorphous phase after grinding and enlarged surface area improved the initial discharge capacity by extending the contact area between the electrolyte and *o*-$LiMnO_2$ particle powders.

However, cycling test of the *o*-$LiMnO_2$ before and after grinding suggested one more interesting fact to us, which is a big difference of the discharge capacity depending on the tested voltage regions. Fig. 10 shows

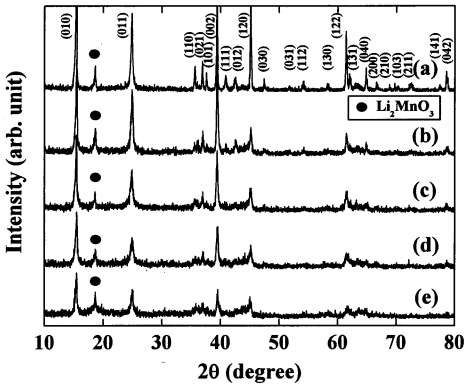

Fig. 9. XRD patterns of $LiMnO_2$ material before and after grinding; (a) 0 h, (b) 6 h, (c) 12 h, (d) 18 h, and (e) 24 h.

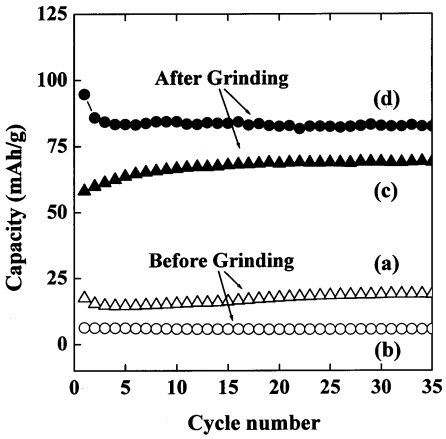

Fig. 10. The plot of specific discharge capacity vs. number of cycles for the Li/1 M $LiPF_6$-EC/DMC/$LiMnO_2$ cells; (a, c) 4 V test, (b, d) 3 V test. Cycling was carried out at a constant charge–discharge current density of 0.4 mA cm^{-2} between 2.2 and 3.6 V for the 3 V test (3.0 and 4.3 V for the 4 V test).

the discharge capacity as a function of cycle number for Li/$LiMnO_2$ cell before and after grinding in the different voltage regions. The charge–discharge current density was 0.4 mA cm^{-2} with a voltage of 2.0–3.6 V for the 3 V test (or 3.0–4.3 V for the 4 V test). The two Li/$LiMnO_2$ cells before grinding commonly showed very small discharge capacity about 5–15 mA h g^{-1} in the 3 and the 4 V region, respectively. The discharge capacity of *o*-$LiMnO_2$ before grinding in the 4 V region was larger than that in the 3 V region, although the difference of capacity was very small. On the other hand, the result of cycling test for the Li/$LiMnO_2$ cells after grinding (Fig. 10c and d) caused one question why the Li/$LiMnO_2$ cells after grinding showed the opposite cycling performance compared with that of *o*-$LiMnO_2$ before grinding; the capacity in the 4 V region was smaller than that in the 3 V region. We suggest one interesting point here, if the improved discharge capacity of *o*-$LiMnO_2$ resulted only from the enlarged specific surface area of powders after grinding, it is a natural consideration that the discharge capacity in the both voltage regions should exhibit the same cycling behavior, regardless of grinding, which the capacity in the 4 V region might be larger than that in the 3 V region after grinding (or the capacity in both voltage regions might exhibit the similar capacity increasing). However, the *o*-$LiMnO_2$ before grinding in the 3 V region initially delivers a discharge capacity of 6.3 mA h g^{-1} and the first discharge capacity after 12 h grinding was 94.7 mA h g^{-1}. The increased capacity of *o*-$LiMnO_2$ in the 3 V region was 15 times as large as that after grinding, while the discharge capacity of *o*-$LiMnO_2$ after grinding in the 4 V region was increased the only 3.3 times that of before grinding. This indication is very interesting to note the grinding treatment may induce the different

electrochemical reaction of o-$LiMnO_2$ material depending on the tested voltage regions.

To investigate the effect of grinding, we measured the cyclic voltamograms of o-$LiMnO_2$ before and after grinding. The potential was scanned at a scan rate of 0.2 mV s^{-1} between 2.0 and 4.5 V. Fig. 11a shows the typical electrochemical reaction of $LiMnO_2$ before grinding, which displayed concrete an oxidation peak at 3.95 V and a very small reduction peak at 2.80 V. It seems there is almost no electrochemical reaction in the 3 V region. However, for the $LiMnO_2$ after 12 h grinding, it exhibits two concrete reaction peaks of the oxidation–reduction process, respectively. Specially, the reduction peak at 2.85 V is remarkably increased after grinding and differentiated clearly from that of the original $LiMnO_2$ compound. From the CV result, we could know the remarkable improvement of capacity in the 3 V region resulted from the activation of lithium insertion of $LiMnO_2$ structure. Recently, Kang and Goodenough's group also reported that lithium manganese oxospinel was remarkably improved cycling performance in the 3 V region after ball milling. They concluded that the role of ball-milling process in lithium manganese oxospinel was the formation of nanometer scale grain, generation of lattice strain, and the change of partial change of oxidation of manganese ions. We also found the formation nano particle grain and strain using TEM analysis. However, o-$LiMnO_2$ material in this study showed no big difference of oxidation of Mn ions between before and after grinding process. The overall compositions were $Li_{0.98}MnO_{2.04}$ for 2 h grinding and $Li_{0.97}MnO_{2.07}$ for 5 h grinding. Therefore, we concluded that the increase of discharge capacity of $LiMnO_2$ material in the 3 V region did not result from the change of oxidation state of Mn ions in this study.

Fig. 12 shows the plot of specific discharge capacity versus number of cycles for the Li/$LiMnO_2$ cell after a 12 h grinding. To prevent excess lithium extraction from the $LiMnO_2$ structure during cycling, the cutoff voltage

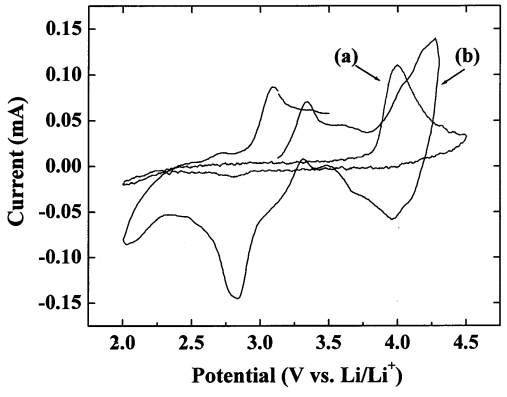

Fig. 11. Cyclic voltamogram of $LiMnO_2$ material, (a) before grinding; (b) after a 12 h grinding. The scan rate was 0.2 mV s^{-1} between 2.0 and 4.5 V at 25 °C.

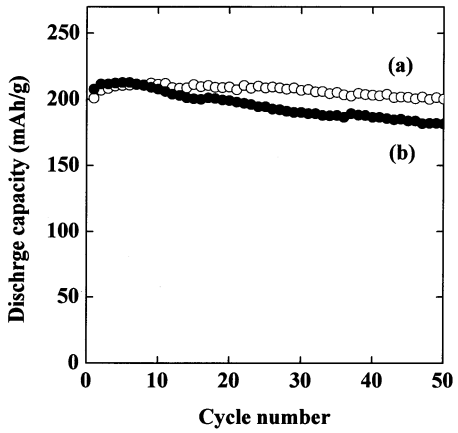

Fig. 12. The plot of specific discharge capacity vs. number of cycles for the Li/1 M $LiPF_6$-EC/DMC/$LiMnO_2$ cells after a 12 h grinding; (a) 25 °C test, (b) 50 °C test. Cycling was carried out at a constant charge–discharge current density of 0.4 mA cm^{-2} between 4.3 and 2.0 V.

was controlled between 4.3 and 2.0 V. As expected, the Li/$LiMnO_2$ cell showed a very high initial discharge capacity of 201 mA h g^{-1} and still delivered 200 mA h g^{-1} after 50 cycles at room temperature. The difference in the initial capacity between before and after grinding at room temperature is about 172 mA h g^{-1}. Although the cycle retention rate of $LiMnO_2$ after grinding decreased to 87% in the high temperature test, it still exhibited a pretty good cycle performance up to 50 cycles. We believe that transition metal-doped $LiMnO_2$ ($LiM_xMn_{1-x}O_2$) with maintaining an orthorhombic structure is one way to improve the high temperature performance of o-$LiMnO_2$ compound.

4. Conclusion

Orthorhombic $LiMnO_2$ was synthesized using LiOH and γ-MnOOH starting materials at 1000–1050 °C in an argon flow by quenching method. XRD revealed that the compound showed an orthorhombic phase of a space group with *Pmnm*. The compound was composed of particles of about 5–15 μm diameter with a bar-shape and small spherical one of about 1–2 μm. We found that the initial discharge capacity of $LiMnO_2$ agreed well with its specific surface area by BET analysis. Furthermore, we firstly revealed that the grinding treatment resulted in activating the lithium insertion–extraction reaction into the $LiMnO_2$ structure in the 3 V region. The Li/$LiMnO_2$ cell before grinding showed a very small initial discharge capacity of about 34 mA h g^{-1} at room temperature. However, after 12 h grinding, the $LiMnO_2$ delivered 201 mA h g^{-1} in the first cycle and still delivered 200 mA h g^{-1} after 50 cycles at room temperature. We concluded that the grinding treatment was a very effective method to increase an initial

discharge capacity of the $LiMnO_2$ compound obtained using quenching method, which accelerated the rapid reaction between the particles and electrolyte at room temperature.

Acknowledgements

The author would like to gratefully thank Mr. Isono of Saga University for powder analysis and Mr. Fukumoto of the Investigation Technology Center of Saga for BET analysis.

References

[1] M. Armand, in: D.W. Murphy, J. Broodhead, B.C.H. Steele (Eds.), Materials for Advanced Batteries, Plenum Press, New York, 1980, p. 145.
[2] B. di Pietro, M. Patriarca, B. Scrosati, J. Power Sources 8 (1982) 289.
[3] Sony lithium ion battery performance summary, JEC Batt. Newsletter 2 (1994) 31.
[4] K. Mizushima, P.C. Jones, P.J. Wiseman, J.B. Goodenough, Mater. Res. Bull. 15 (1980) 783.
[5] J.R. Dahn, U. Von Sacken, C.A. Michel, Solid State Ionics 44 (1990) 87.
[6] D. Guyomard, J.M. Tarascon, Solid State Ionics 69 (1994) 222.
[7] R.J. Gummow, D.C. Liles, M.M. Thackeray, Mater. Res. Bull. 28 (1993) 1249.
[8] A.R. Armstrong, P.G. Bruce, Nature 381 (1996) 499.
[9] M. Okada, T. Mouri, M. Yoshio, Abstract of the 1999 Joint International Meeting, Hawaii 99, 1999, pp. 327.
[10] W.D. Johnston, R.R. Keikes, J. Am. Chem. Soc. 78 (1956) 3255.
[11] R. Hoppe, G. Brachtel, M. Jansen, Z. Anorg. Allg. Chem. 417 (1975) 1.
[12] T. Ohzuku, A. Ueda, T. Hirai, Chem. Express 7 (1992) 193.
[13] N. Reimers, E.W. Fuller, E. Rossen, J.R. Dahn, J. Electrochem. Soc. 140 (1993) 3396.
[14] M. Tabuchi, C. Ado, Masquelier, I. Matsubara, H. Sakaebe, H. Kageyama, H. Kobayashi, R. Kanno, O. Nakamura, Solid State Ionics 89 (1996) 53.
[15] S.T. Myung, S. Komaba, N. Kumagai, Chem. Lett. (2001) 80.
[16] P. Strobel, J.P. Levy, J. Cryst. Growth 66 (1984) 257.
[17] R.J. Gummow, M.M. Thackeray, J. Electrochem. Soc. 141 (1994) 1178.
[18] L. Croguennec, P. Deniard, R. Brec, A. Lecerf, J. Mater. Chem. 5 (1995) 1919.
[19] L. Croguennec, P. Deniard, R. Brec, P. Biensan, M. Broussely, Solid State Ionics 89 (1996) 197.
[20] L. Croguennec, P. Deniard, R. Brec, J. Electrochem. Soc. 144 (1997) 3323.
[21] W. Tang, H. Kanoh, K. Ooi, J. Solid State Chem. 142 (1999) 19.
[22] I.J. Davidson, R.S. McMillan, J.J. Murray, J.E. Greedan, J. Power Sources 54 (1995) 232.
[23] Y.I. Jang, B. Huang, H. Wang, D.R. Sadoway, Y.M. Chiang, J. Electrochem. Soc. 146 (1999) 3217.
[24] Y.M. Chiang, D.R. Sadoway, Y.I. Jang, B. Huang, H. Wang, Electrochem. Solid-State Lett. 2 (1999) 1.
[25] Y.S. Lee, M. Yoshio, Electrochem. Solid-State Lett. 4 (10) (2001) A166.
[26] Y. Xia, M. Yoshio, J. Power Sources 57 (1995) 125.
[27] H. Hayakawa, T. Takada, H. Enoki, E. Akiba, J. Mater. Sci. Lett. 17 (1998) 811.
[28] J.M. Tarascon, W.R. Mckinnon, F. Coowar, T.N. Bowmer, G. Amatucci, D. Guyomard, J. Electrochem. Soc. 141 (1994) 1421.
[29] M. Yoshio, H. Noguchi, T. Miyashita, H. Nakamura, A. Kozawa, J. Power Sources 54 (1995) 483.
[30] Y.S. Lee, C.S. Yoon, Y.K. Sun, M. Yoshio, Electrochem. Solid-State Lett. 5 (1) (2002) A1.
[31] J. Kim, A. Manthiram, Electrochem. Solid-State Lett. 2 (2) (1999) 55.
[32] J. Kim, A. Manthiram, Nature 390 (1997) 265.
[33] S.H. Kang, J.B. Goodenough, L. Rabenberg, Chem. Mater. 13 (2001) 1758.